Path-Following Controller Designs for Autonomous and Semi-Autonomous Industrial Motor Graders

Anthony Beca
Ingenuity Labs Research Institute
Queen's University
Kingston, Ontario, Canada
anthony.beca@queensu.ca

Joshua A. Marshall
Ingenuity Labs Research Institute
Queen's University
Kingston, Ontario, Canada
0000-0002-7736-7981

***Abstract*—Haulage road maintenance is crucial for operational efficiency and safety in mining and construction activities. Industrial motor graders play a key role in this task, both on surface and in underground mines, where production vehicles—such as trucks and loaders—are increasingly being driven autonomously. However, motor graders have yet to be commercially automated. The redundant kinematics of motor graders, including articulation, front-axle steering, and blade operations, pose technical challenges for autonomy. In this work, we leverage the steering redundancy of motor grader designs to formulate a new path following controller that is compatible with existing approaches for the automation of articulated vehicles. The proposed methodology, coined "Single-Track Control" (STC) allows for coordination of both the front-axle steering angle and the vehicle's articulation angle to keep the front and rear wheels on a common track. This innovation mitigates the risk of collisions with drift walls and improves manoeuvrability. It can be used for semi-autonomous operations, to reduce the complexity for operators, as well as for fully autonomous operations. The approach was validated in simulation, comparing the implementation performance of two controller types.**

***Index Terms*—Mining robotics, Autonomous driving, Path-following control, Nonlinear control**

I. Introduction

Automated road maintenance is a central challenge for mining sites the employ automated or tele-operated machinery. If road conditions deteriorate, autonomous zones are often shut down to allow a manual operator to restore road quality. As the scale and frequency of robotic mining operations increases [1], the need to address robotic grading becomes more dire. Unlike centre-articulated vehicles such as load-haul-dump (LHD) and haulage trucks [1], [2], industrial motor graders (e.g., see Fig. 1) pose unique challenges due to their usage and design. Indeed, some factors include steering redundancy, six-degree-of-freedom (6-DoF) blade control, and complex environment interactions, all of which hinder potential integration into existing automation frameworks.

As such, this paper proposes Single-Track Control (STC): a control methodology that leverages the kinematic redundancy of a motor grader to emulate the path-following behaviour of an ideal centre-articulated vehicle. The benefits of STC are threefold: 1) existing automation techniques for centre-articulated vehicles can be directly applied to motor graders, with low-level controllers tracking the equivalent inputs for a desired articulation angle; 2) integration with vehicle controls consolidates steering as a single input, decreasing the need for specialized operator training in semi-autonomous mode; and 3) improved safety and manoeuvrability by ensuring that the rear wheels follow the same path as the front wheels, mitigating the risk of collisions with drift (tunnel) walls.

This research was funded in part by the Natural Sciences and Engineering Research Council of Canada (NSERC) under the NSERC Canadian Robotics Network (NCRN) grant number NETGP 508451-17.

Fig. 1: MacLean Engineering GR5 grader is a purpose-built machine for road surface maintenance in mining applications. The vehicle can be steered both by turning the front-axle wheels as well as by hydraulically actuating the angle of an articulation joint that connects the front and rear components of the machine [Photo source: macleanengineering.com].

II. Related Work

This section presents some background and work related to the problem of autonomous grading.

A. Autonomous Grading

Literature on the automation of motor graders is scarce. The dearth of such research is in part due to the complexity of the task, in conjunction with the difficulty of simulation and of data collection from real vehicles. Furthermore, most existing work focuses on the path-following automation of surface

grading due to GPS signal availability and a comparatively simpler operating environment. For instance, [3] designed and simulated a Pure Pursuit controller for front-wheel steering motor graders, modelled as a tricycle. Similarly, [4] conducted field testing of a Pure Pursuit controller. To match the desired curvature, and resolve kinematic redundancy, the method actuates articulation only when the front-wheel steering is not sufficient, which is not viable for underground grading because it could lead to collisions with the walls of the drift.

B. Articulated Vehicles

We can look to underground path-following automation for articulated vehicles for prior work, with commercial implementation of LHDs in use at mine sites [1]. For example, [2] describes the system design and implementation of autonomous LHDs, applying a PD-controller to feedback linearized error dynamics. The approach was extended for Iterative-Learning-Control to compensate for model uncertainties in [5]. Furthermore, steering geometry analysis for centre-articulated vehicles has been well studied [6], unlike graders.

C. Kinematically Redundant Industrial Vehicles

In other industries, the path-following automation of kinematically redundant industrial vehicles has been studied. Most relevant are front-wheel steering vehicles with completely unactuated (i.e., passive) articulation. For example, Non-Linear Model Predictive Control (NMPC) has been used for truck-trailer systems [7]. Agricultural vehicles with implements [8] have used Frenet frames to estimate lateral and heading errors with respect to the utility point of the implement.

III. Method Design

This paper formulates a relationship between front-wheel steering and articulation angle to functionally obtain the path-tracking behaviour of an "ideal" centre-articulated vehicle. An "ideal" centre-articulated vehicle is one where the front and rear wheels follow the same path, thus allowing for maximum manoeuvrability in tight spaces such as in underground mines. The work presented in this paper allows existing automation approaches (e.g., localization and path planning algorithms) designed for centre-articulated vehicles to be directly extended to motor graders and further provides the advantage that the front and real wheels of the grader can be made to track the exact same path, which has practical advantages for underground applications. We formulate the Single Track Control (STC) relationship for graders by analyzing the steering geometry (Section III-A), and implement controllers by deriving the motor grader kinematics (Section III-B) and feedback linearized error dynamics (Section III-C).

A. Single Track Control

Single-track path following behaviour is desired for mining applications because the front and rear wheels will follow the same path. Thus, if an operator can enter a drift (tunnel), the rear component of the vehicle will also not collide with the wall. However, as seen in Fig. 1, the front component length is nearly four times as long as the rear component—standard for motor graders.

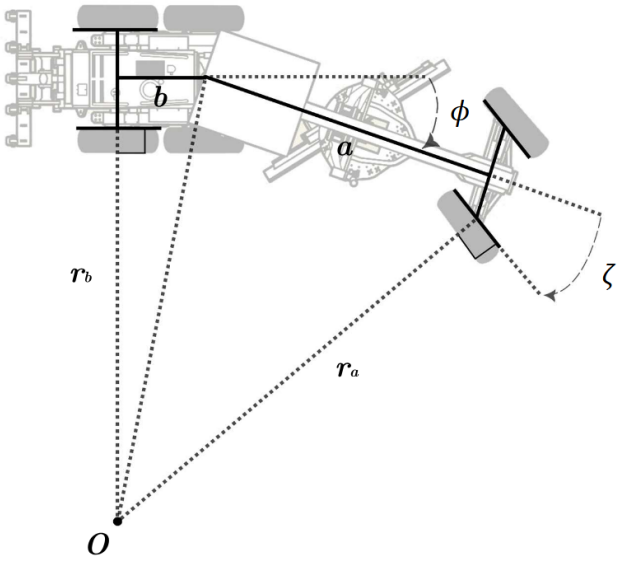

Fig. 2: Steering geometry of the grader: a and b are the component lengths, ϕ and ζ represent articulation joint angle and steering angle, respectively.

Fig. 5 shows the traced track (centroid of front and rear axles) for a simulated motor grader under three different steering modes: 1) using the articulation joint for steering; 2) steering the front wheels to turn; and 3) by using Single Track Control. As can be seen in the figure, there is a lateral gap between the STC-disabled controllers, posing a risk for collisions with drift walls when turning. In contrast, the trace for both axles with STC are aligned, and the turning radius is tighter then when using each input independently.

To obtain the STC behaviour, we found a relationship for the articulation angle ϕ and front-wheel steering angle ζ (see Fig. 2) for turning radii $r_a > 0$, $r_b > 0$ within the physical limits of the configuration. Derived expressions for the turning radii were obtained by using techniques applied to articulated vehicles in [6], given by

$$r_a = \frac{b + a\cos\phi}{\sin(\phi+\zeta)} \tag{1}$$

$$r_b = \frac{b\cos(\phi+\zeta) + a\cos\zeta}{\sin(\phi+\zeta)}, \tag{2}$$

where $a > 0$ and $b > 0$ denote the lengths of the front and rear components, respectively. To obtain STC, we impose

$$r_a = r_b \tag{3}$$

$$\frac{b + a\cos\phi}{\sin(\phi+\zeta)} = \frac{b\cos(\phi+\zeta) + a\cos\zeta}{\sin(\phi+\zeta)} \tag{4}$$

$$\frac{b}{a} = \frac{\cos\phi - \cos\zeta}{\cos(\phi+\zeta) - 1}. \tag{5}$$

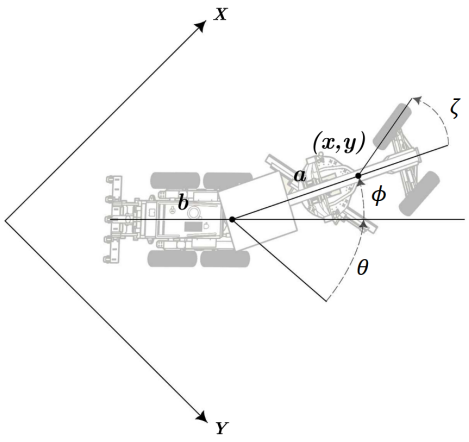

Fig. 3: Kinematic model of the motor grader, with component lengths a and b, heading angle θ, articulation angle ϕ, and front-wheel steering angle ζ.

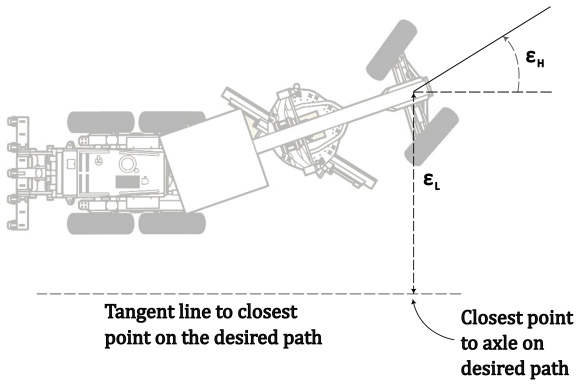

Fig. 4: Error definitions for path following with respect to the tangent line to the desired path to be followed.

It turns out that the constraint equation (5) is not separable as a function of only the articulation angle ϕ or the steering angle ζ, thus a numerical method is needed to solve this equation.

A controller is used to determine a desired articulation angle ϕ_d with respect to lateral and heading errors, then the corresponding desired steering angle ζ_d is approached iteratively. We vary ϕ because motor graders typically a have greater range of motion for front wheel steering, $\pm 55°$, than for the articulation angle, $\pm 35°$. This way, the smallest total turning radius possible with STC is achieved.

In summary, to follow a given path, the articulation angle ϕ is varied to track heading error, as if the grader were a centre-articulated vehicle, and the desired front-wheel steering angle ζ is solved to satisfy (5). Bisection Search was employed as a numerical method to converge to ζ, for its robustness to initial conditions and guaranteed convergence to an approximation.

B. Vehicle Kinematics

A kinematic model of the grader is formulated by deriving the nonholonomic constraints of a simplified model, shown as Fig. 3. The configuration space is given by $(x, y) \in \mathbb{R}^2$ in Cartesian space, heading of rear component $\theta \in \mathbb{S}^1$, articulation angle $\phi \in [\phi_{\min}, \phi_{\max}]$, and front wheel steering angle $\zeta \in [\zeta_{\min}, \zeta_{\max}]$, encoded as

$$\mathbf{q} = (x, y, \theta, \phi, \zeta) \in \mathbf{Q} \tag{6}$$

$$\mathbf{Q} = \mathbb{R}^2 \times \mathbb{S}^1 \times [\phi_{\min}, \phi_{\max}] \times [\zeta_{\min}, \zeta_{\max}], \tag{7}$$

with the body fixed coordinate system (x, y) selected at the centre of the front axle (see Fig. 3).

The vehicle is constrained to not move (i.e., no slip) in the directions perpendicular to the direction of each set of wheels. Although rough terrain conditions can result in a violation of the no-slip condition, this paper serves as a proof of concept and leaves it for future work to increase the fidelity of the vehicle model. In any case, graders large weight, slow speeds, and 6-wheeled configuration mitigate slip, while large terrain interaction forces represent a larger challenge.

These nonholonomic constraints are given by

$$\begin{aligned}\mathbf{A}(\mathbf{q}) &= \begin{bmatrix}\omega_F^\top & \omega_R^\top\end{bmatrix} \\ &= \begin{bmatrix} -\sin(\theta+\phi+\zeta) & -\sin\theta \\ -\cos(\theta+\phi+\zeta) & \cos\theta \\ 0 & -a\cos\phi - b \\ 0 & -a\cos\phi \\ 0 & 0 \end{bmatrix}.\end{aligned} \tag{8}$$

There are three control inputs available to a grader operator: linear speed v_1, articulation rate v_2, and front wheel steering rate v_3, denoted together as $\mathbf{v} \in \mathbb{R}^3$. We wish to obtain vector fields $\{\mathbf{g}_1, \mathbf{g}_2, \mathbf{g}_3\}$ that annihilate constraints (8), thus providing directions for v_1, v_2, and v_3. Setting $\mathbf{g}_i \perp \omega_j$, the kinematics are computed to be

$$\dot{\mathbf{q}} = \begin{bmatrix}\dot{x}\\ \dot{y}\\ \dot{\theta}\\ \dot{\phi}\\ \dot{\zeta}\end{bmatrix} = \begin{bmatrix} \cos(\theta+\phi+\zeta) & 0 & 0 \\ \sin(\theta+\phi+\zeta) & 0 & 0 \\ \frac{\sin(\phi+\zeta)}{a\cos\phi+b} & \frac{-a\cos\phi}{a\cos\phi+b} & 0 \\ 0 & 1 & 0 \\ 0 & 0 & 1 \end{bmatrix} \begin{bmatrix} v_1 \\ v_2 \\ v_3 \end{bmatrix}. \tag{9}$$

Note that any basis can be chosen, but this model is unique for our choice of inputs.

C. Feedback Linearized Error Dynamics

To achieve path following we adapt existing techniques for the automated path following of articulated vehicles [2], feedback linearized [9] error dynamics are derived. As shown in Fig. 4, two errors are regulated with respect to the front wheels: lateral ε_L and heading ε_H error.

In the body fixed coordinate frame, ε_L is given as y, and ε_H is given as the heading of the front wheels

$$\begin{aligned}\varepsilon_L &:= (\varepsilon_L)_F = y \\ \varepsilon_H &:= (\varepsilon_H)_F = \theta + \phi + \zeta,\end{aligned} \tag{10}$$

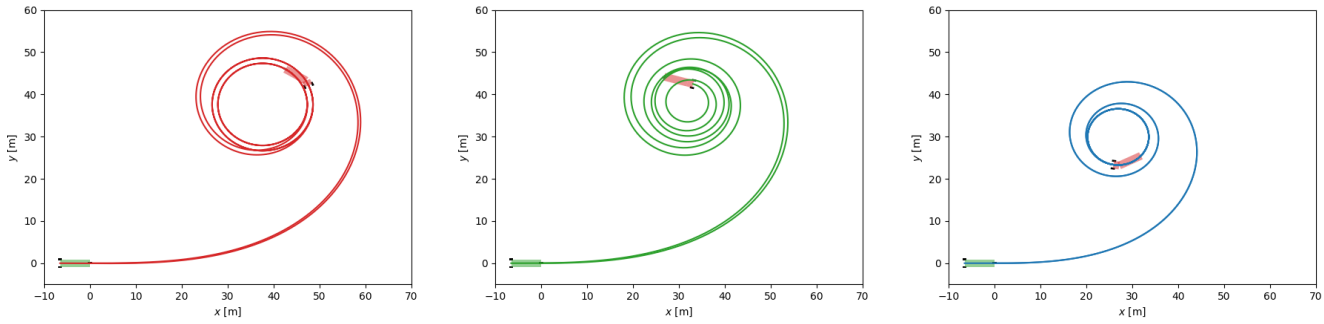

Fig. 5: Track traces for maximum articulation (left), maximum steering (centre), and single-track control with maximum articulation (right). Traces indicate the path of the centroid of each axle. Control input is incremented monotonically.

and the error dynamics are computed to be

$$\begin{aligned}\dot{\varepsilon}_L &= \dot{y} = v_1 \sin\varepsilon_H \\ \dot{\varepsilon}_H &= \dot{\theta} + \dot{\phi} + \dot{\zeta} \\ &= v_1 \frac{\sin(\phi+\zeta)}{a\cos\phi + b} + v_2\left(1 - \frac{a\cos\phi}{a\cos\phi+b}\right) + v_3.\end{aligned} \tag{11}$$

A nonlinear change of coordinates to $\mathbf{z} = (z_1, z_2)$ for feedback linearization (FBL) is introduced as

$$z_1 := \varepsilon_L \tag{12}$$

$$z_2 := \dot{\varepsilon}_L = v_1 \sin\varepsilon_H. \tag{13}$$

Taking the derivative yields the new error dynamics

$$\dot{z}_1 := z_2 \tag{14}$$

$$\begin{aligned}\dot{z}_2 &:= v_1 \dot{\varepsilon}_H \cos\varepsilon_H \\ &= v_1\left(v_1 \frac{\sin(\phi+\zeta)}{a\cos\phi+b} + v_2\left(1 - \frac{a\cos\phi}{a\cos\phi+b}\right) + v_3\right)\cos\varepsilon_H.\end{aligned} \tag{15}$$

In matrix form, the FBL error dynamics are

$$\begin{bmatrix}\dot{z}_1 \\ \dot{z}_2\end{bmatrix} = \begin{bmatrix}\dot{\varepsilon}_L \\ \ddot{\varepsilon}_L\end{bmatrix} = \underbrace{\begin{bmatrix}0 & 1 \\ 0 & 0\end{bmatrix}}_{\mathbf{A}}\mathbf{z} + \underbrace{\begin{bmatrix}0 \\ 1\end{bmatrix}}_{\mathbf{B}}\eta. \tag{16}$$

Hence, it is clear that $\dot{z}_2 = \eta$. This FBL error system can be stabilized with any suitable linear controller.

D. Controller Designs

In this work, proportional-derivative (FBL+PD) and Model Predictive Control (FBL+MPC) controllers were tested in simulation with and without STC in discrete time. For each, the vehicle speed v_1 was held constant, η was calculated as a control input, used to determine articulation rate v_2, then STC was applied to obtain a desired steering angle, $\zeta_{d,k+1}$, tracked with a first order lower-level controller. Here $k \in \mathbb{N}$ is the time step such that $t = kT$ and $T > 0$ the sample time [s], and d indicates a desired value.

1) FBL+PD: We use a controller of the form

$$\eta = \mathbf{K}\mathbf{z} = \begin{bmatrix}k_1 & k_2\end{bmatrix}\begin{bmatrix}z_1 \\ z_2\end{bmatrix} \tag{17}$$

to asymptotically stabilize the error dynamics for $k_1, k_2 < 0$ [2]. Equation (17) can be rearranged for v_2 (via (15)) as

$$v_2 = \frac{b}{a\cos\phi + b}\left(\frac{\eta}{v_1\cos\varepsilon_H} - \frac{v_1\sin\phi}{a\cos\phi+b}\right). \tag{18}$$

Note that dependence on front wheel steering input, v_3 is omitted because it is tracked by the STC control loop.

2) FBL+MPC Formulation: Based on prior work [10] for FBL+MPC of differential drive vehicles, the error dynamics (14), (15) are approximated in discrete time as

$$\mathbf{z}_{k+1} = \mathbf{F}\mathbf{z}_k + \mathbf{G}\eta_k = \begin{bmatrix}1 & T \\ 0 & 1\end{bmatrix}\mathbf{z}_k + \begin{bmatrix}\frac{T^2}{2} \\ T\end{bmatrix}\eta_k. \tag{19}$$

We define control input u_k as

$$\mathbf{u}_k = (\eta_k, \eta_{k+1}, ..., \eta_{k+p-1}), \tag{20}$$

where $p \in \mathbb{Z}_+$ is the prediction time horizon in k discrete steps. The discrete time integration of the control sequence is

$$\mathbf{u}_k = \Delta\mathbf{u}_k + \mathbf{u}_{k-1} = (\Delta\eta_k, \Delta\eta_{k+1}, ..., \Delta\eta_{k+p-1}). \tag{21}$$

We use the FBL states $\mathbf{z}_k$ as predicted values to be minimized given the sequence of FBL control inputs $\mathbf{u}_k$. By minimizing FBL states over the prediction horizon p, we also minimize path following errors. Taken over the prediction horizon, the FBL states are stacked together such that

$$\mathbf{y}_{k+1} = \Delta\mathbf{y}_{k+1} + \mathbf{y}_k = (\mathbf{z}_{k+1}, \mathbf{z}_{k+2}, \ldots, \mathbf{z}_{k+p}) \tag{22}$$

thus the change in FBL states at each timestep k is

$$\Delta\mathbf{y}_{k+1} = (\Delta\mathbf{z}_{k+1}, \Delta\mathbf{z}_{k+2}, \ldots, \Delta\mathbf{z}_{k+p}). \tag{23}$$

We can use these relationships to describe the FBL states over the prediction horizon as

$$\underbrace{\begin{bmatrix}\Delta\mathbf{z}_{k+1} \\ \Delta\mathbf{z}_{k+2} \\ \vdots \\ \Delta\mathbf{z}_{k+p}\end{bmatrix}}_{\Delta\mathbf{y}_{k+1}} = \underbrace{\begin{bmatrix}\mathbf{F} \\ \mathbf{F}^2 \\ \vdots \\ \mathbf{F}^p\end{bmatrix}}_{\mathbf{L}}\Delta\mathbf{z}_k + \underbrace{\begin{bmatrix}\mathbf{G} & \mathbf{0} & \cdots & \mathbf{0} \\ \mathbf{F}\mathbf{G} & \mathbf{G} & \cdots & \mathbf{0} \\ \vdots & \vdots & \ddots & \vdots \\ \mathbf{F}^{p-1}\mathbf{G} & \mathbf{F}^{p-2}\mathbf{G} & \cdots & \mathbf{G}\end{bmatrix}}_{\mathbf{M}}\underbrace{\begin{bmatrix}\Delta\eta_k \\ \Delta\eta_{k+1} \\ \vdots \\ \Delta\eta_{k+p-1}\end{bmatrix}}_{\Delta\mathbf{u}_k},$$

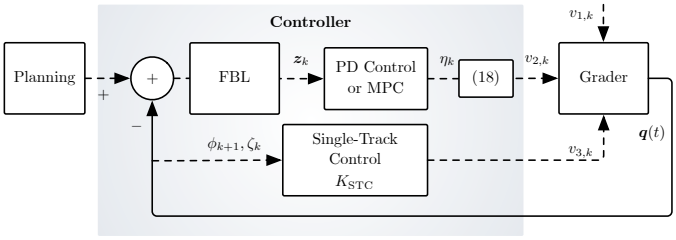

Fig. 6: System block diagram showing STC in parallel with path-following control (either PD or MPC).

written compactly as

$$\Delta \mathbf{y}_{k+1} = \mathbf{L}\Delta \mathbf{z}_k + \mathbf{M}\Delta u_k. \tag{24}$$

Note that, in this case, matrices $\mathbf{L}$ and $\mathbf{M}$ depend solely on $\mathbf{F}$ and $\mathbf{G}$. Thus, $\mathbf{L}$ and $\mathbf{M}$ can be precomputed.

3) FBL+MPC Cost Functions: Two cost functions were implemented to contrast performance. Optimization 1 weighs the magnitude of change in control input, whereas Optimization 2 weighs the magnitude of the input [10]. The weighted cost functions are given as

$$J_1(\Delta \mathbf{u}_k) = \mathbf{y}_{k+1}^\top \mathbf{Q}\mathbf{y}_{k+1} + \Delta \mathbf{u}_k{}^\top \mathbf{R}\Delta \mathbf{u}_k, \tag{25}$$
$$J_2(\Delta \mathbf{u}_k) = \mathbf{y}_{k+1}^\top \mathbf{Q}\mathbf{y}_{k+1} + \mathbf{u}_k{}^\top \mathbf{R}\mathbf{u}_k, \tag{26}$$

Since these cost functions are quadratic, representing a linear convex optimization problem, optimal inputs $\Delta \mathbf{u}_k^*$ are obtained by finding the global minimum per

$$\frac{\partial J(\cdot)}{\partial \mathbf{u}} = 0.$$

Optimal control inputs are given as

$$J_1(\Delta \mathbf{u}_k) \Rightarrow \tag{27}$$
$$\Delta \mathbf{u}_k^* = -(\mathbf{M}^\top \mathbf{Q}\mathbf{M} + \mathbf{R})^{-1}\mathbf{M}^\top \mathbf{Q}(\mathbf{y}_k + \mathbf{L}\Delta \mathbf{z}_k),$$
$$J_2(\Delta \mathbf{u}_k) \Rightarrow \tag{28}$$
$$\Delta \mathbf{u}_k^* = -(\mathbf{M}^\top \mathbf{Q}\mathbf{M} + \mathbf{R})^{-1}(\mathbf{M}^\top \mathbf{Q}(\mathbf{y}_k + \mathbf{L}\Delta \mathbf{z}_k) + \mathbf{R}\mathbf{u}_{k-1}).$$

A system block diagram illustrating the control design is provided in Fig. 6. Feedback linearized error dynamics (11) converge to zero with a PD or MPC controller, used to set the articulation input, $v_{2,k}$ (18), while a first-order controller tracks the desired steering angle to satisfy the Single-Track Control condition (5) with steering input $v_{3,k}$.

E. Simulation Experiments

A Python simulation environment was developed to evaluate and tune the STC+FBL controllers. To compare steady-state performance and controller responsiveness, a step-input path was used as a test case. Each controller was tested under identical initial conditions, with vehicle parameters chosen to approximate those of a real underground grader (see Table I). Many real-world factors were not considered – although controller performance would certainly be impacted, the purpose of this work is to demonstrate that Single-Track Control is feasible to apply to motor graders.

TABLE I: Simulation parameters and vehicle physical parameters chosen to approximate those of a real underground grader.

Controller	Parameter(s)	Value
All Controllers	Front component length, a	5.26 m
	Rear component length, b	1.27 m
	Steering range	$\pm 55°$
	Articulation range	$\pm 35°$
	$\mathbf{q}_0$	$[0\text{ m}, 10\text{ m}, 0°, 0°, 0°]$
	Vehicle speed	5 m/s
	Waypoint resolution	0.5 m
	Time step, T	0.1 s
STC+FBL+PD	natural frequency, ω_n	$\in [0, 2.5]$
	damping ratio, ζ	$\in [0, 2.5]$
	n_{samples}	1000
STC+FBL+MPC	$\mathbf{q}$	$\in [0, 50]$
	$\mathbf{r}$	$\in [0, 10]$
	p	4 / T
	n_{samples}	100

IV. Simulation Results

A. Observed Effect of STC on System Behaviour

Feedback linearization (FBL) "linearizes" the system by counteracting nonlinear terms through a carefully designed control input. However, its effectiveness is limited when there is a plant-model mismatch, potentially leading to failure or oscillations [11]. In this study, FBL is used to compute the articulation angle for an idealized articulated vehicle. The computed input is applied, and the steering angle is determined separately. As a result, the steering input is omitted from the FBL system, introducing unmodelled behaviours.

Fig. 7 compares the performance of the STC+FBL+PD controller for four values of k_{STC}, increasing from left to right. As can be seen for $k_{\text{STC}} = 0$, there is a smooth transition from high-error, low-effort performance to low-error, high-effort performance. This result is intuitive, as the more aggressive the inputs are, the more responsive the controller is to path-following errors. In contrast, the rightmost figure, for $k_{\text{STC}} = 1$ exhibits two distinct regions—a stable region (low-effort), and a highly oscillatory (high-effort) region. This result is caused by the aforementioned plant-model mismatch, introducing nonlinear terms that are not cancelled by the FBL error dynamics. Notice that the boundary between the regions of control effort can be moved by varying k_{STC}. This is an expected result because the gain directly varies the magnitude of the unmodelled system behaviour.

B. Tuning Study

Several strategies can mitigate the oscillatory effects caused by the plant-model mismatch: namely, 1) rate limits can be inputs on control inputs, reflective of hardware limitations on real graders, and 2) bifurcation analysis can be performed to quantify the parametric uncertainty over the operating range, informing tuning [12]. While promising, these methods are beyond the scope for this work.

Thus, to gain intuition on the performance of the controllers, random sampling was used to effectively span the parameter space to inform tuning strategies. Samples were generated via Latin Hypercube Sampling, a statistical method that randomly

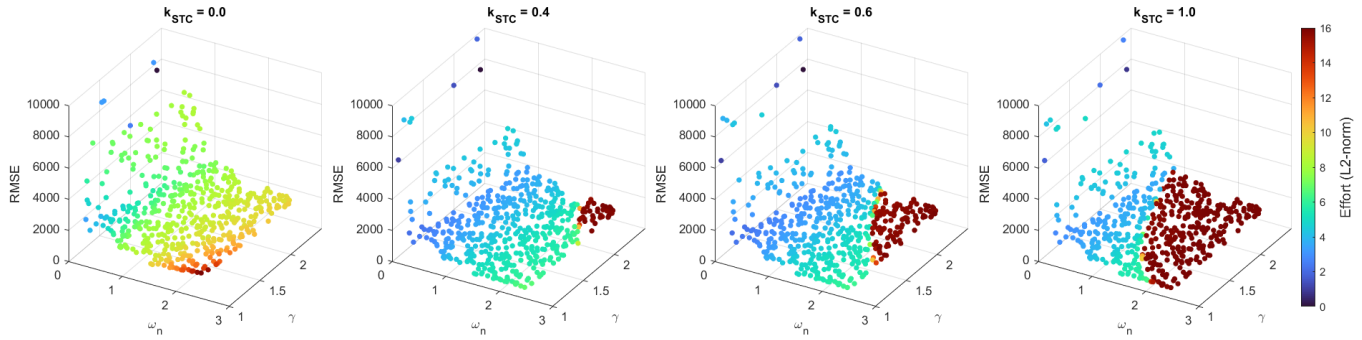

Fig. 7: Comparison of STC+FBL+PD controllers for four values of k_{STC}. Colour indicates control effort (L^2 norm) of inputs, and z-axis indicates root mean squared path-tracking errors.

TABLE II: Comparison of controllers. Error was measured as RMSE of lateral and heading path following errors (ε_L and ε_H); effort was measured as the L^2 norm of the articulation rate input (v_2).

Controller	k_{STC}	Parameters	RMSE	Effort
STC+FBL+PD	0.0	$\omega_n = 1.63$, $\zeta = 1.03$	1310	6.19
	0.4	$\omega_n = 1.63$, $\zeta = 1.03$	678	5.70
	0.6	$\omega_n = 1.63$, $\zeta = 1.03$	672	5.63
	1.0	$\omega_n = 1.63$, $\zeta = 1.03$	668	5.50
STC+FBL+MPC1	0.0	$q = 22.7$, $r = 1.89$	580	2.97
	0.4	$q = 11.4$, $r = 4.29$	614	2.34
	0.6	$q = 11.4$, $r = 4.29$	622	2.34
	1.0	$q = 11.4$, $r = 4.29$	635	2.67
STC+FBL+MPC2	0.0	$q = 2.16$, $r = 4.78$	465	3.35
	0.4	$q = 0.239$, $r = 5.19$	478	2.51
	0.6	$q = 0.239$, $r = 5.19$	478	2.49
	1.0	$q = 0.239$, $r = 5.19$	477	2.46

distributes points within a stratified grid, ensuring uniform coverage across all dimensions, and reducing clustering compared to other methods [13]. Sampling ranges and number of samples were determined from experimentation to explore a domain of values with stable path following performance, outlined in Table I. Further work could extend this approach to explore the nine-dimensional parameter space of the STC+FBL+MPC controllers, varying look-ahead horizon and penalty weights for each state and control elements.

To maximize performance for practical applications, careful tuning must be done to avoid the region of instability. When applied to a real grader, unmodelled dynamics from actuators and environment interaction will necessitate conservative tuning parameters to mitigate high oscillations. For the STC+FBL+PD controller, Fig. 7 suggests a critically damped system ($\zeta = 1$), a small value for $k_{\mathrm{STC}} \approx 0.4$ to maximize the region of stability, and to increase ω_n until the desired performance is achieved. For both STC+FBL+MPC controllers, it is recommended to maintain of $\frac{q}{r} \approx 5$ for best performance. It is observed that k_{STC} has a small effect on performance for the MPC controllers (see Table II).

C. Controller Performance

The performance of each controller was assessed based on two primary criteria: Path-following accuracy, measured by RMSE of lateral and heading errors, as well as control effort, defined as the sum of the L^2 norm of both varying control inputs, v_2 and v_3, representing the total actuator energy required to follow the reference path.

For each controller, Table II shows the metrics for "good" gains, obtained by following the tuning strategy outlined in IV-B. For consistent comparison, identical gains were used to compare each of the controllers that include STC ($k_{\mathrm{STC}} > 0$). Because the loss landscape is different for STC-disabled controllers, separate "good" gains were chosen. Fig. 8 compares the path tracking performance for each controller, while Fig. 9 show the magnitude of control inputs.

For the STC+FBL+PD controller, the best results in terms of RMSE and control effort were observed with $k_{\mathrm{STC}} = 1$. However, as evident in Fig. 7 the region of instability is much greater than for other values, without a major improvement in performance (> 5 % for both metrics). Additionally, it is apparent that STC-enabled controllers demonstrated improved performance over the STC-disabled controller in both metrics.

With MPC controllers, the STC-disabled trials demonstrated lower path-tracking error and higher control effort than the next best STC-enabled controller (MPC1: -6 % RMSE, $+24$ % effort, MPC2: -3 % RMSE, $+36$ % effort). This may be attributed to the plant-model mismatch induced by STC, affecting the performance of the FBL controller to track $v_{2,k}$.

Best performance for MPC1 was observed with $k_{\mathrm{STC}} = 0.4$, representing a small improvement over $k_{\mathrm{STC}} = 0.6$. High oscillations were observed with $k_{\mathrm{STC}} = 1.0$, as seen in Fig. 8 and 9, indicating instability. All STC-enabled MPC2 controllers demonstrated nearly-identical RMSE and control effort (within 2 % each), indicating that STC has minimal impact on controller performance for MPC2.

Among STC-enabled controllers, MPC1 showed the lowest control effort overall. This makes sense because $J_1(\Delta \mathbf{u}_k)$ is defined as penalizing the magnitude of the change in input over each timestep, per (25). Additionally, STC-enabled MPC2 showed the lowest RMSE. This is expected because $J_2(\Delta \mathbf{u}_k)$ is defined to minimize control input magnitude, instead rewarding convergence to the path, per (25). As expected, both MPC controllers outperform the PD controller in terms of RMSE and effort, but are more computationally expensive.

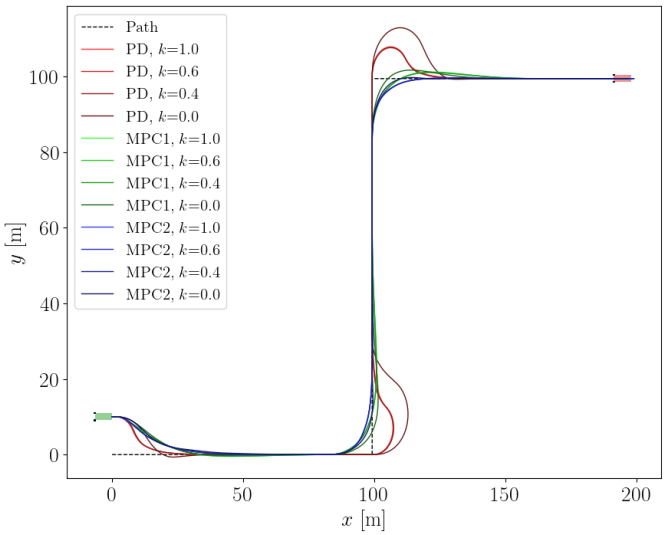

Fig. 8: Path following trace for each controller.

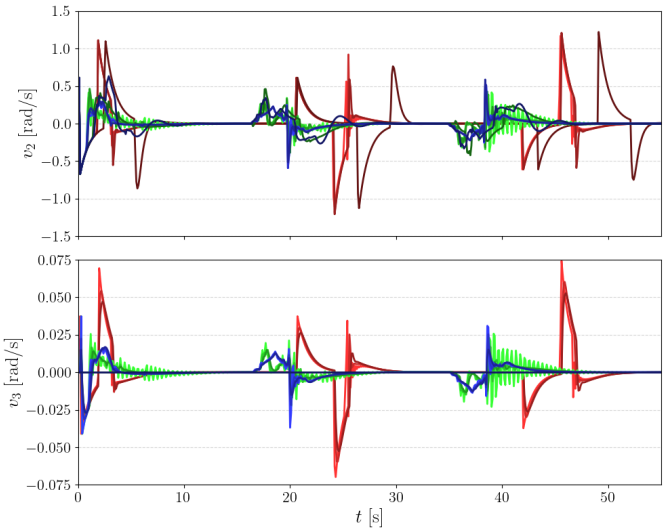

Fig. 9: Magnitude of articulation and steering inputs for each controller.

D. Recommendation

STC-enabled MPC2 controllers demonstrate the most potential for implementation on a real vehicle. With the lowest path tracking error, low control effort, and stability for all k_{STC}, there is lower risk for collisions with drift walls.

Although PD controllers are the simplest to implement, the large region of instability as well as delays in changing direction are practical considerations that limits its usefulness. Furthermore, the STC-enabled MPC1 controllers presented the lowest control effort, but can be unstable for high values of k_{STC}, behaviour that could be amplified when slip, friction, noise, and other effects affect the system.

E. Future Work

Several areas for further research and application remain open. One key direction is addressing the plant-model mismatch, which could be mitigated by imposing actuator rate limits to reflect real-world hardware constraints, conducting bifurcation analysis to quantify performance across the operating range, or a modification to the FBL error dynamics to explicitly account for STC effects. Additionally, practical implementation requires a deeper understanding of how to model and compensate for dynamic disturbances that arise from terrain-interaction forces. Furthermore, incorporating wheel lean as an additional control input within STC could further enhance stability by actively managing lateral forces, a potential avenue to improve manoeuvrability.

V. Conclusion

This paper formulates Single Track Control (STC) for motor graders, leveraging kinematic redundancy to ensure that the front and rear wheels follow a single track. Three controllers were implemented, PD as well as two MPC, for feedback linearized error dynamics. Simulation experiments were conducted to validate path-following control, which revealed a bisection of control effort into regions of low-and-high stability for similar path tracking performance. The boundary of this bisection could be varied by changing the first-order gain on STC, k_{STC}, without compromising path tracking errors. The results of simulation experiments indicate that STC-enabled MPC2 controllers are the most practical for real-world implementation. Stable for all values of k_{STC}, and demonstrating the best performance (28 % lower RMSE than next best), is the best candidate for undeground motor grader autonomy.

References

[1] J. A. Marshall, A. Bonchis, E. M. Nebot, and S. Scheding, "Robotics in mining," in *Springer Handbook of Robotics*, 2nd ed., B. Siciliano and O. Khatib, Eds. Springer, Cham, 2016, ch. 59, pp. 1549–1576.

[2] J. A. Marshall, T. D. Barfoot, and J. Larsson, "Autonomous underground tramming for center-articulated vehicles," *Journal of Field Robotics*, vol. 25, pp. 400–421, 06 2008.

[3] R. Y. Sukharev, "Pure pursuit method use to control unmanned motor grader," *The Russian Automobile and Highway Industry Journal*, vol. 19, no. 2, p. 156–169, May 2022.

[4] R. Nasrallah and S. Cetikunt, "Steer-by-wire control system using GPS for articulated vehicles," *Fault Tolerant Drive By Wire Systems: Impact on Vehicle Safety and Reliability*, 2012.

[5] L. Dekker, "Industrial-scale autonomous vehicle path following by feedback linearized iterative learning control," Master's thesis, Queen's University, 2018.

[6] P. Corke and P. Ridley, "Steering kinematics for a center-articulated mobile robot," *IEEE Transactions on Robotics and Automation*, vol. 17, no. 2, pp. 215–218, 2001.

[7] M. Lukassek, J. Dahlmann, A. Völz, and K. Graichen, "Model predictive path-following control for truck–trailer systems with specific guidance points — design and experimental validation," *Mechatronics*, vol. 100, p. 103190, 2024.

[8] M. Lukassek, A. Völz, T. Szabo, and K. Graichen, "Model predictive control for agricultural machines with implements," in *Proceedings of the 2020 28th Mediterranean Conference on Control and Automation (MED)*, 2020, pp. 387–392.

[9] H. K. Khalil, *Nonlinear Systems*, 3rd ed. Upper Saddle River, NJ: Prentice Hall, 2002.

[10] J. Wang, M. T. H. Fader, and J. A. Marshall, "Learning-based model predictive control for improved mobile robot path following using gaussian processes and feedback linearization," *Journal of Field Robotics*, vol. 40, no. 5, pp. 1014–1033, 2023.
[11] S. B. da Cunha, "On the robustness of feedback linearization," *International Journal of Dynamics and Control*, vol. 12, pp. 3318–3331, 2024.
[12] J. Hahn, M. Mönnigmann, and W. Marquardt, "Robust tuning of feedback linearizing controllers via bifurcation analysis," *IFAC Proceedings Volumes*, vol. 37, no. 1, pp. 475–480, 2004, 7th International Symposium on Advanced Control of Chemical Processes (ADCHEM 2003), Hong-Kong, 11-14 January 2004.
[13] C. Song and R. Kawai, "Monte carlo and variance reduction methods for structural reliability analysis: A comprehensive review," *Probabilistic Engineering Mechanics*, vol. 73, p. 103479, 2023.